

ResLT: Residual Learning for Long-tailed Recognition

Jiequan Cui ¹ Shu Liu ² Zhuotao Tian ¹ Zhisheng Zhong ¹ Jiaya Jia ^{1,2}

¹The Chinese University of Hong Kong ²SmartMore

{jqcui, zttian, leo{jia}@cse.cuhk.edu.hk, liushuhust@gmail.com}

Abstract

Deep learning algorithms face great challenges with long-tailed data distribution which, however, is quite a common case in real-world scenarios. Previous methods tackle the problem from either the aspect of input space (re-sampling classes with different frequencies) or loss space (re-weighting classes with different weights), suffering from heavy over-fitting to tail classes or hard optimization during training. To alleviate these issues, we propose a more fundamental perspective for long-tailed recognition, i.e., from the aspect of parameter space, and aims to preserve specific capacity for classes with low frequencies. From this perspective, the trivial solution utilizes different branches for the head, medium, tail classes respectively, and then sums their outputs as the final results is not feasible. Instead, we design the effective residual fusion mechanism – with one main branch optimized to recognize images from all classes, another two residual branches are gradually fused and optimized to enhance images from medium+tail classes and tail classes respectively. Then the branches are aggregated into final results by additive shortcuts. We test our method on several benchmarks, i.e., long-tailed version of CIFAR-10, CIFAR-100, Places, ImageNet, and iNaturalist 2018. Experimental results manifest that our method achieves new state-of-the-art for long-tailed recognition. Code will be available at <https://github.com/FPNAS/ResLT>.

1. Introduction

Convolutional neural networks (CNNs) have achieved impressive success on various tasks, including large-scale image classification [21, 31, 33, 13], object detection [27] and semantic segmentation [7]. The incredible progress stems in part from high-quality and large-scale datasets, such as ImageNet [28], MS COCO [24] and Places [44]. These datasets are carefully designed with balanced distributions over different classes. In real-world applications, data could follow an unexpected long-tailed distribution where only a few head classes and a large number of tail classes exist. The long-tailed phenomenon may lead to se-

vere degradation of performance for all models that do not take it into consideration. We in this paper address long-tailed recognition, *i.e.*, recognition on data with long-tailed distributions.

One of the greatest challenges in the long-tailed setting is data imbalance. It is also the principal reason for head classes dominating the training procedure, making head classes enjoy much higher accuracy than tail classes. In the literature, two kinds of methods tackle the long-tailed problem via re-sampling and re-weighting [1, 16, 8, 12, 6, 29]. It is found that over-sampling tail-class images [29, 42, 2, 3] may still suffer from heavy over-fitting to tail classes while under-sampling by dropping a large number of head-class images [12, 18, 2] inevitably impairs the generalization ability of deep models. Also, for re-weighting methods, previous works [14, 15] have demonstrated that re-weighting strategies may cause optimization difficulties during training on large-scale and real-world datasets.

Regarding procedures, re-sampling re-balances head and tail classes in input space by constructing balanced mini-batches during the course of training as shown in Fig. 1(a). Differently, re-weighting deals with the loss space by assigning different weights for classes according to the respective numbers of samples as shown in Fig. 1(b). Albeit the procedural difference, we note that these two lines, by nature, both *alter model parameters* to adjust tail classes response. This finding leads to our key idea of *re-balancing in parameter space directly*.

Our direct operations on the head and tail classes regarding parameter space can avoid heavy over-fitting to tail classes and the difficult optimization problem mentioned above. To illustrate that designing these effective operations is nontrivial, we show in Fig. 1(c) a naive solution. It preserves specialized parameters for the head, medium, and tail classes respectively via three branches of \mathcal{N}_h , \mathcal{N}_m and \mathcal{N}_t . The branches are optimized for respective recognition and the final result is obtained by summing outputs of them. Unfortunately, this naive solution does not work well in experiments.

Contrary to these naive operations, we model the long-

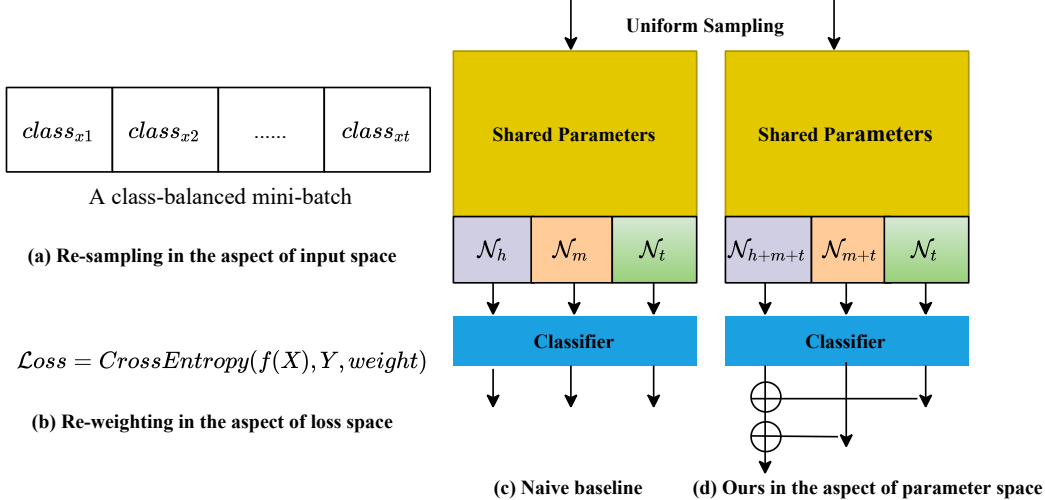


Figure 1: Comparison between our method and previous ones. Previous re-sampling and re-weighting balance input space and loss space respectively, with effect on the model parameters. Our method is built regarding the most fundamental parameter space, individually preserves specialized parameters for head, medium and tail classes with three sub-branches. These sub-branches are combined finally to enhance classification results of tail and medium classes by the proposed residual fusion mechanism. In (b), (X, Y) is a batch of images and their corresponding labels. $weight$ represents a vector of class-wise weights which usually is in reverse proportion to the number of samples of classes. Classifier is a shared fc layer among the three branches in (c) and (d).

tailed recognition problem as one residual learning process and propose a novel residual fusion mechanism, as shown in Fig. 1(d). It has one main branch (\mathcal{N}_{h+m+t}) optimized to classify images of all classes while the other two residual branches (\mathcal{N}_{m+t} and \mathcal{N}_t) are optimized to recognize images in medium+tail and tail classes respectively. Outputs of these three branches is aggregated into the final result by additive shortcuts.

An intuitive explanation of our strategy is to gradually enhance classification results on tail classes with other learned residual branches. It is noteworthy that samples belonging to the head, medium, and tail classes still dominate \mathcal{N}_{h+m+t} , \mathcal{N}_{m+t} and \mathcal{N}_t individually in the training procedure, and thus guarantee parameter specialization of the head, medium and tail classes.

We extensively validate our method on several long-tailed benchmark datasets using long-tailed versions of CIFAR-10, CIFAR-100, ImageNet, Places, and iNaturalist 2018 data. Experimental results manifest that our method yields new state-of-the-art for long-tailed recognition. Our key contributions are as follows.

- We study the problem from a new perspective of parameter space that leads to an effective re-balance between head and tail classes in the long-tailed setting.
- We propose the residual fusion mechanism, making re-balance in the aspect of parameter space feasible and

alleviating limitations in previous works.

- We validate our method on representative benchmarks and accomplish new state-of-the-art (SOTA). Note that this is the first time that a one-stage method consistently surpasses two-stage methods on long-tailed CIFAR-10, CIFAR-100, ImageNet, iNaturalist 2018 all these datasets.

2. Related Work

Re-sampling Strategy There are two groups of re-sampling strategies: over-sampling the tail-class images [29, 42, 2, 3] and under-sampling the head-class images [12, 18, 2]. Over-sampling is regularly useful on large datasets and often suffers from heavy over-fitting to tail classes especially on small datasets. For under-sampling, it discards a large portion of data, which inevitably causes degradation of the generalization ability of deep models. Moreover, the under-sampling strategy is not suitable when data is largely imbalanced.

Re-weighting Strategy Re-weighting [14, 15, 36, 26, 30, 17] is another prominent strategy. It assigns different weights for classes and even samples. The vanilla re-weighting method gives class weights in reverse proportion to the number of samples of classes. However, with large-scale data, re-weighting makes the deep models difficult to

optimize during training [14, 15]. Cui et al. [8] relieved the problem using "effective numbers" to calculate class weights.

Another line of work is to adaptively re-weight each sample. Focal loss [23] assigned smaller weights for well-classified samples. Li et al. [22] down-weighted samples with very small or large gradients in response to the principle that samples with small gradients are usually well-classified and samples with large gradients are usually out of the distribution.

Two-stage Methods Cao et al. [4] first observed that re-weighting and re-sampling are inferior to the vanilla empirical risk minimization (ERM) algorithm before annealing the learning rate. A two-stage deferred re-balancing optimization schedule was proposed, which trains using vanilla ERM with the LDAM loss before annealing learning rate, and then deploys a re-weighted LDAM loss with a much smaller learning rate.

Recently, Kang et al. [20] and Zhou et al. [43] concluded that although class re-balance strategies matter when jointly training representation and classifier, uniform sampling gives more general representations. Based on this observation, Kang et al. [20] achieved state-of-the-art results on long-tailed ImageNet (ImageNet-LT) by decomposing representation and classifier learning, *i.e.*, first train the deep models with uniform sampling, then fine-tune the classifier with class-balanced sampling while keeping parameters of representation learning fixed. Similarly, Zhou et al. [43] integrated *mixup* into the proposed cumulative learning strategy with which they bridged the representation learning and classifier re-balancing and achieved state-of-the-art results on long-tailed CIFAR (CIFAR-LT) and iNaturalist 2018.

The two-stage design clearly defies the end-to-end merit that we used to believe since the deep learning era. But why does the two-stage training outperform the end-to-end one largely in long-tailed classification? The concurrent work [34], which is also a one-stage method, analyzed the reason from the perspective of causal graph and concluded that the bad momentum causal effects played a vital role. Differently, we address the problem in terms of residual learning.

3. Our Method

Motivation As illustrated in Fig. 1(a), re-sampling strategies build class-balanced mini-batch data for training. However, over-sampling tail-class images is easy to get into trouble of heavy over-fitting to tail classes while under-sampling head-class images hurts the generalization ability of deep models due to discarding a large number of head-class images that are conducive in learning good representations. For re-weighting methods, previous works [14, 15] demonstrate that it makes deep models difficult to optimize. We, unlike these solutions, explore another way to re-balance

regarding parameter space directly, avoiding above disadvantages and making further improvements.

Table 1: Top-1 accuracy (%) of baselines on CIFAR-10-LT with the imbalance factor 0.02. ResNet-32 is adopted.

Method	head	medium	tail	All
Baseline (CE)	97.10	83.10	70.01	78.50
Baseline-1	97.30	76.65	45.20	61.91
Baseline-2	97.40	80.40	41.05	62.20
Baseline-3	91.65	60.90	63.63	68.69
ResLT (Ours)	95.70	75.95	81.45	83.46

3.1. Re-balancing in Parameter Space

We are the first to propose re-balancing regarding parameter space. To understand the difficulty, we show a naive way by preserving several specialized parameters for the head, medium, tail classes separately by three branches (*i.e.*, \mathcal{N}_h , \mathcal{N}_m , and \mathcal{N}_t). They are shown in Fig. 1(c). After sorting regarding the number of images, all the classes are divided into 3 groups for the head, medium, tail classes, and we guarantee that the three groups have the same imbalance factor β . $\beta = \frac{N_{min}}{N_{max}}$ where N_{max} and N_{min} are the numbers of training samples for the most frequent class and the least frequent class in each group. Under this case, the core issue is the way to fuse the outputs of these branches into the final prediction because it is impossible to know whether one image belongs to head or medium or tail classes at inference time. Therefore, fusing the three branches is not trivial. Here we compare three straightforward fusion methods with the basic vanilla baseline with cross-entropy. They are set as follows.

- (1): $\arg \max \{ \max \text{Concat}\{\mathcal{N}_h(x), \mathcal{N}_m(x), \mathcal{N}_t(x)\} \}$
- (2): $\arg \max \{ \mathcal{N}_h(x) + \mathcal{N}_m(x) + \mathcal{N}_t(x) \}$
- (3): $\arg \max \{ \sigma(\mathcal{N}_h(x)) + \sigma(\mathcal{N}_m(x)) + \sigma(\mathcal{N}_t(x)) \}$

$\mathcal{N}_h(x)$, $\mathcal{N}_m(x)$ and $\mathcal{N}_t(x)$ represent output of three branches before softmax function taking image x as input. *Concat* represents the "torch.cat" operation in Pytorch. For baseline (1), we first *Concat* $\mathcal{N}_h(x)$, $\mathcal{N}_m(x)$, $\mathcal{N}_t(x)$ and apply max operation both in the second dimension. σ is the softmax function. The experimental results are summarized in the Table 1. It shows that these straightforward fusion methods do not work satisfactorily and even yield inferior results compared to the vanilla baseline. We instead propose an effective residual fusion mechanism to handle this challenging issue.

3.2. Residual Fusion Mechanism

Under the long-tailed setting, models usually achieve high accuracy on head classes while the performance on tail

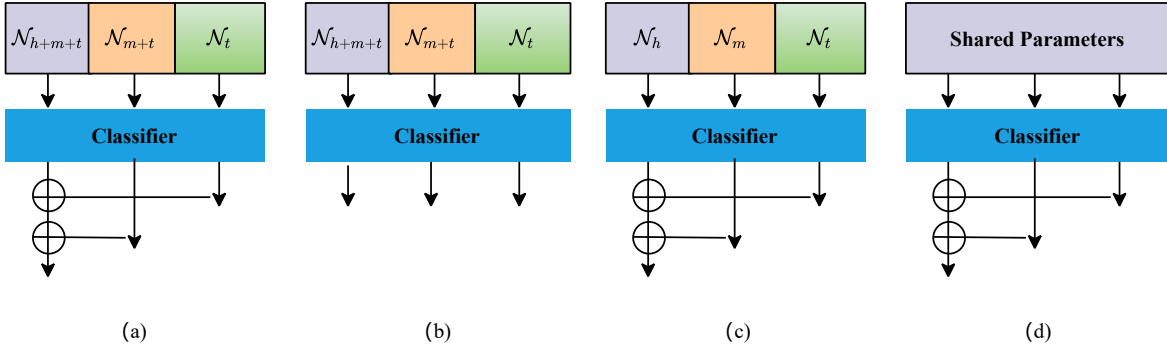


Figure 2: Ablation study for the residual fusion and parameter specialization mechanisms. (a) is our proposed residual fusion module while (b) and (c) are variants of (a). For (b), there is no additive shortcut, different from (a). For (c), the three branches have no residual relationship – nested class assignments, unlike (a). (d) is without parameter specialization mechanism.

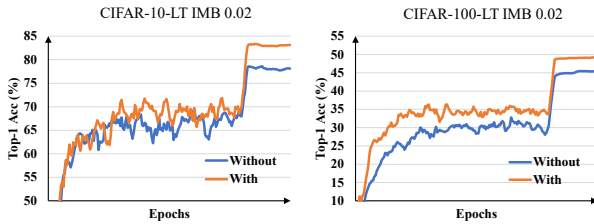


Figure 3: Importance of parameter specialization.

classes is unsatisfactory. Based on this phenomenon, we model the long-tailed recognition problem as one residual learning process. It uses extra learned residual branches to enhance classification results on tail classes. Here we clear that the "residual" denotes the nested class assignments for different branches in our method.

As shown in Fig. 1(d), the model parameters are divided into two parts: shared and specialized parameters. Shared parameters are for common features across all the classes while specialized parameters are to preserve specific capacity for the head, medium, tail classes with three branches \mathcal{N}_{h+m+t} , \mathcal{N}_{m+t} and \mathcal{N}_t correspondingly. In fact, the three branch networks are implemented by only one extra 1×1 grouped convolution with group number 3. Though only a few parameters are introduced, this parameter specialization mechanism plays an important role as demonstrated in Sec. 3.3.1 with experimental verification.

To effectively aggregate the three branches, we propose the residual fusion module shown in Fig. 1(d). We model the long-tailed recognition problem as such residual learning process where one main branch \mathcal{N}_{h+m+t} learns to recognize images of all the classes and the other two residual branches \mathcal{N}_{m+t} , \mathcal{N}_t are used to classify medium+tail classes and tail classes respectively. The outputs of the three branches are added together as the final result. It is worth noting that head, medium, and tail classes still dominate

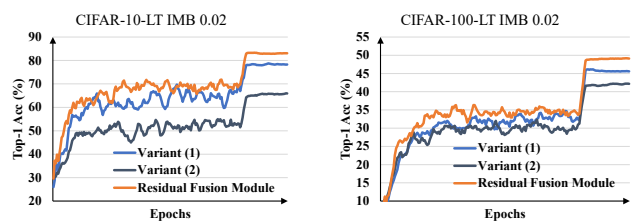


Figure 4: Residual fusion module analysis.

branches \mathcal{N}_{h+m+t} , \mathcal{N}_{m+t} , \mathcal{N}_t respectively, and thus the parameter specialization of these classes are preserved.

In our residual fusion mechanism, loss functions are deployed in training process as

$$\mathcal{L}_{fusion} = \mathcal{J}(\mathcal{N}_{h+m+t}(X) + \mathcal{N}_{m+t}(X) + \mathcal{N}_t(X), Y) \quad (1)$$

$$\mathcal{L}_{branch} = \sum_{i \in \{h+m+t, m+t, t\}} \mathcal{J}(N_i(SX_i), SY_i) \quad (2)$$

$$\mathcal{L}_{all} = (1 - \alpha) \mathcal{L}_{fusion} + \alpha \mathcal{L}_{branch} \quad (3)$$

where (X, Y) denotes the uniformly sampled images and labels of a mini-batch. (SX_{h+m+t}, SY_{h+m+t}) is the same as (X, Y) consisting of all class images. (SX_{m+t}, SY_{m+t}) is a subset of (X, Y) only containing images of medium and tail classes. (SX_t, SY_t) is a subset of (X, Y) only containing images belonging to tail classes. \mathcal{J} is cross-entropy loss and α is a hyper-parameter.

The fusion loss item \mathcal{L}_{fusion} in Eq. (1) optimizes for all the classes. The outputs of branches \mathcal{N}_{m+t} and \mathcal{N}_t are added to the outputs of main branch \mathcal{N}_{h+m+t} to obtain the fused outputs. Therefore, during inference, we just sum outputs of the three branches as the final result. The branch-independent loss item \mathcal{L}_{branch} in Eq. (2) is for \mathcal{N}_{h+m+t} , \mathcal{N}_{m+t} and \mathcal{N}_t respectively, further encouraging parameter specialization for head, medium, and tail classes respectively. \mathcal{L}_{all} is our final loss which is a weighted sum of \mathcal{L}_{fusion} and \mathcal{L}_{branch} with a trade-off hyper-parameter α .

3.3. Analysis of Our Method

Our method depends on two key components: parameter specialization and residual mechanism. Here we analyze each of them with extensive experiments.

3.3.1 Importance of Parameter Specialization

Though the three sub-branches are implemented by only a 1×1 grouped convolution with group number 3, we show that it is important to reserve specialized parameters for head, medium and tail classes. We compare strategies with and without the parameter specialization mechanism on CIFAR-10-LT and CIFAR-100-LT with the imbalance factor 0.02. For the setting without parameter specialization, as shown in Fig. 2(d), we let outputs of the three branches be the same while keeping the same loss functions in Eqs. (1), (2) and (3) in implementation. As shown in Fig. 3, the model with the parameter specialization mechanism yields much higher accuracy than the model without it, which manifests the vast importance of our parameter specialization mechanism.

3.3.2 Analysis of Residual Fusion Module

To further study the proposed residual fusion mechanism, we conduct ablation study to understand the role of each component in our residual fusion module by comparing its two variants on CIFAR-10-LT and CIFAR-100-LT with the imbalance factor 0.02:

- Possible variant (1): as shown in Fig. 2(b), we remove the additive shortcuts from our designed residual fusion module. During inference, we take the output of main branch \mathcal{N}_{h+m+t} as the final results. The branches \mathcal{N}_{m+t} and \mathcal{N}_t only play the role of regularization during training.
- Possible variant (2): as shown in Fig. 2(c), we remove the residual relationship among the three branches. \mathcal{N}_h , \mathcal{N}_m and \mathcal{N}_t are optimized to classify images of head, medium and tail classes respectively.

As shown in Fig. 4, it is clear that both the variants (1) and (2) yield lower performance than our full residual fusion module. This phenomenon demonstrates that the residual relationship (nested class assignments) among branch networks and the additive shortcuts are two core factors that make it feasible to solve long-tailed recognition in parameter space. Moreover, it shows the fundamental difference between our proposed residual learning mechanism and previous work [13].

Comparison with Re-weighting Our method may reminiscent attentive readers of re-weighting methods consider-

ing that the loss with respect to tail-class images is calculated by three branches while the loss for head-class images is calculated by only \mathcal{N}_{h+m+t} branch. In fact, the comparison between the structure of Fig. 2(a) and the structure of Fig. 2(c) in Sec. 3.3.2 has validated that the improvements come from our residual mechanism instead of such naive re-weighting. Here we further clarify some fundamental differences between our method and re-weighting.

We explicitly preserve specific capacity for the head, medium, tail classes. Besides, re-weighting independently pre-defines scalar factors as the class weights simply according to the number of images in the class while our method adaptively enhances classification results of tail classes with the learned residual branches of \mathcal{N}_{m+t} and \mathcal{N}_t . Further, our method captures the important relationship between different classes within each branch.

4. Experiments

4.1. Datasets and Experimental Setting

CIFAR-10-LT and CIFAR-100-LT datasets CIFAR-10 and CIFAR-100 both have 60,000 images – 50,000 for training and 10,000 for validation with 10 categories and 100 categories respectively. For a fair comparison, we use the long-tailed versions of CIFAR datasets with the same setting as those used in [4, 43]. They control the degrees of data imbalance with an imbalance factor β . $\beta = \frac{N_{min}}{N_{max}}$ where N_{max} and N_{min} are the numbers of training samples for the most frequent class and the least frequent class. Following [43], we conduct experiments with imbalance factors 0.01, 0.02, and 0.1.

ImageNet-LT and Places-LT ImageNet-LT and Places-LT were proposed in [25] by Liu et.al. ImageNet-LT is a long-tailed version of the large-scale object classification dataset ImageNet [28] by sampling a subset following the Pareto distribution with power value $\alpha=6$. It contains 115.8K images from 1,000 categories, with class cardinality ranging from 5 to 1,280. Places-LT is a long-tailed version of the large-scale scene classification dataset Places [44]. It consists of 184.5K images from 365 categories with class cardinality ranging from 5 to 4,980.

iNaturalist 2018 The iNaturalist 2018 [35] is one species classification dataset, which is on a large scale and suffers from extremely imbalanced label distributions. It is composed of 437.5K images from 8,142 categories. In addition to the extreme imbalance, iNaturalist 2018 dataset also confronts the fine-grained problem [37].

Evaluation Protocol Following Liu et al. [25] and Kang et al. [20], on ImageNet-LT, Places-LT and iNaturalist 2018, we further report results on three splits of the set

Table 2: Top-1 accuracy (%) on ImageNet-LT for ResNeXt-50. † denotes results directly copied from [25]. ”§” denotes the model is trained with strong data augmentation (mixup and autoaugment).

Method	One-stage	Many	Medium	Few	All
Baseline(CE)	✓	67.6	42.8	13.4	47.6
Mixup [40]	✓	67.3	41.0	11.1	46.3
Lifted Loss [32] †	✓	41.1	35.4	24.0	35.2
Focal Loss [23] †	✓	41.1	34.8	22.4	34.6
Range Loss [41] †	✓	41.1	35.4	23.2	35.1
τ -normalized [20]	✓	60.9	49.2	36.8	51.5
cRT [20]	✗	63.7	47.6	28.3	50.7
LWS [20]	✗	63.3	48.4	32.0	51.5
ResLT	✓	63.0	50.5	35.5	52.9
ResLT §	✓	63.6	55.7	38.9	56.1

Table 3: Top-1 accuracy (%) on Places-LT for ResNet-152. † denotes results directly copied from [20]. ”§” denotes pre-trained model on ImageNet is trained with strong data augmentation (cutmix) provided by [39].

Method	One-stage	Many	Medium	Few	All
Baseline (CE)	✓	45.7	27.3	8.2	30.2
Lifted Loss [32] †	✓	41.1	35.4	24.0	35.2
Focal Loss [23] †	✓	41.1	34.8	22.4	34.6
Range Loss [41] †	✓	41.1	35.4	23.2	35.1
τ -normalized [20]	✓	37.8	40.7	31.8	37.9
OLTR [25]	✗	44.7	37.0	25.3	35.9
LFME [38]	✗	39.3	39.6	24.2	36.2
NCM [20]	✗	40.4	37.1	27.3	36.4
cRT [20]	✗	42.0	37.6	24.9	36.7
LWS [20]	✗	40.6	39.1	28.6	37.6
ResLT	✓	39.8	43.6	31.4	39.8
ResLT §	✓	40.3	44.4	34.7	41.0

of classes: Many-shot (more than 100 images), Medium-shot ($20 \sim 100$ images) and Few-shot (less than 20 images). More results are provided in the supplementary file.

Training Details For long-tailed CIFAR datasets, we follow [4, 43] to pre-process images. We randomly crop a 32×32 patch from the original image or its horizontal flip with 4 pixels padded on each side and normalize the pixel values into $[0, 1]$. To be consistent with previous setting [4, 44], we adopt ResNet-32 [13] as our backbone network for all experiments. SGD optimizer with momentum 0.9 is adopted. We train all models for 200 epochs for our ResLT method. The initial learning rate is set to 0.1 and the first five epochs are trained with linear warm-up. The learning rate is decayed at the 160 and 180 epochs by 0.1 respectively. The batch size 128 is used through all the experiments.

For a fair comparison, we adopt the same experimental

setting as [20] on ImageNet-LT, Places-LT and iNaturalist 2018. For Places-LT, following previous setting [25, 20], we choose ResNet-152 as the backbone network, pre-train it on the full ImageNet-2012 dataset (provided by torchvision), and finely tune it for 30 epochs on Places-LT. On ImageNet-LT, we report results with ResNet-10, ResNeXt-50 and ResNeXt-101. For consistency with previous setting, ResNet-50 is used for iNaturalist 2018 and we train 200 epochs following [20]. For all experiments, we use SGD optimizer with momentum 0.9 on 4 NVIDIA 2080Ti GPUs. For ResNet-10, ResNet-50, and ResNeXt-50, we adopt cosine learning rate schedule gradually decaying from 0.1 to 0. We use image resolution 224×224 and batch size 256. For ResNet-152 and ResNeXt-101, we adopt cosine learning rate schedule gradually decaying from 0.05 to 0, image resolution 224×224 and batch size 128 for the limited GPU memory.

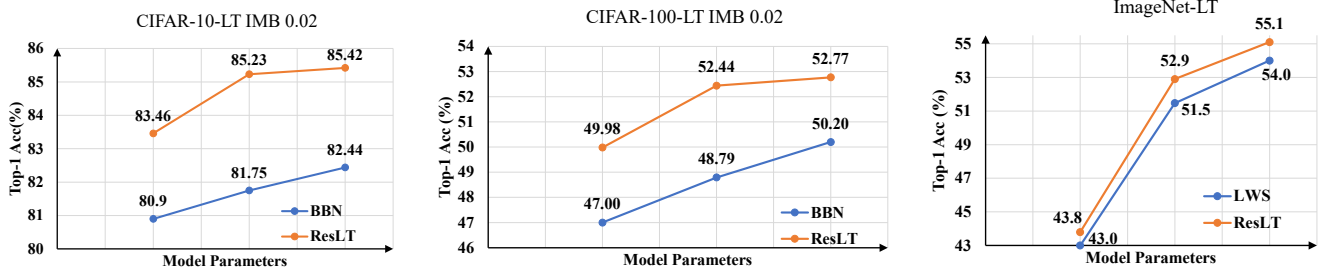


Figure 5: Effects of model size on long-tailed recognition. ResNet-32(1x), ResNet-32(2x), ResNet-32(3x) are used for CIFAR-LT while ResNet-10, ResNeXt-50, ResNeXt-101 are applied for ImageNet-LT.

4.2. Ablation Study

How does the model size affect our method? To go deeper in understanding the effects of model size on long-tailed recognition, we explore various models with different parameters on CIFAR100-LT, CIFAR10-LT with imbalance factor 0.02 and ImageNet-LT datasets. For CIFAR100-LT, CIFAR10-LT, we evaluate ResNet-32(1x), ResNet-32(2x) and ResNet-32(3x). Specifically 1x, 2x, 3x mean the multiplier of channels in each layer. For ImageNet-LT, ResNet-10, ResNeXt-50, ResNeXt-101 are used. As shown in Fig. 5, with the increase of model parameters, Our method can consistently surpass SOTA method BBN on CIFAR-LT and LWS on ImageNet-LT.

How does the hyper-parameter α affect our method? We conduct ablation study on choosing a proper α on CIFAR-10-LT, CIFAR-100-LT with imbalance factor 0.02, and ImageNet-LT datasets. For CIFAR-10-LT and CIFAR-100-LT, $\alpha = 0.9950$ is adopted, while we use 0.99 and 0.90 for ImageNet-LT and iNaturalist 2018 respectively in our experiments. As shown in Fig. 6, even when $\alpha = 1$ that only with \mathcal{L}_{branch} loss in training, the performance is even much better than baselines in Table 1 mentioned in Sec. 3.1, demonstrating the importance of the residual mechanism – nested class assignments for different branches.

How does the number of groups affect our method? Here we have further explored the effects of different number of groups on CIFAR-10-LT, CIFAR-100-LT with imbalance factor 0.01. As shown in Table 4, when the number of groups larger than 3, there is no obvious improvements.

Table 4: Ablation study for different number of groups. “#” represents the number of groups. Top-1 accuracies (%) are reported. We use ResNet-32 as backbone in experiments.

Dataset	#2	#3	#4	#5
CIFAR-10-LT	78.83	80.44	80.80	80.44
CIFAR-100-LT	45.11	45.34	45.34	45.14

4.3. Comparison Methods

In experiments, we compared with two kinds of methods: one-stage methods and state-of-the-art two-stage methods.

- One-stage methods. For one-stage methods, we mainly compare with mixup [40], LDAM [4] and recently proposed BBN [43] methods.
- Two-stage methods. For two-stage methods, we mainly compare with the recently proposed decoupling representation and classifier learning [20].

4.4. Comparison with SOTA On Long-tailed Datasets

Comparison on CIFAR-10-LT and CIFAR-100-LT We conduct extensive experiments on CIFAR-10 and CIFAR-100 with imbalance factors of 0.01, 0.02 and 0.1, same as previous setting [4, 43]. The experimental results are summarized in Table 5. Compared with one-stage methods and two-stage methods, our ResLT outperforms them by a large margin. Specifically, our method outperforms the SOTA method BBN by 2.78%, 2.96% and 1.76% on CIFAR-100-LT with imbalance factors 0.01, 0.02, and 0.1 respectively. On CIFAR-10-LT, we also surpass BBN significantly.

Comparison on ImageNet-LT Table 2 shows experimental results on ImageNet-LT. Here, we mainly compare with the recent SOTA method [20]. We observe that 90 epochs training is not enough to converge for deep models on ImageNet-LT. Under longer training with 180 epochs, the recent SOTA method [20] can be significantly further improved. And we use this strong setting for comparisons. As shown in Table 2, ResNext-50 trained with our ResLT method in an end-to-end fashion enjoys 1.4% higher Top-1 accuracy than [20]. Moreover, as shown in Fig. 5, we also test our method on ResNet-10 and ResNext-101. Our method consistently surpasses LWS [20] by 0.8% ~ 1.4% across small models to large models.

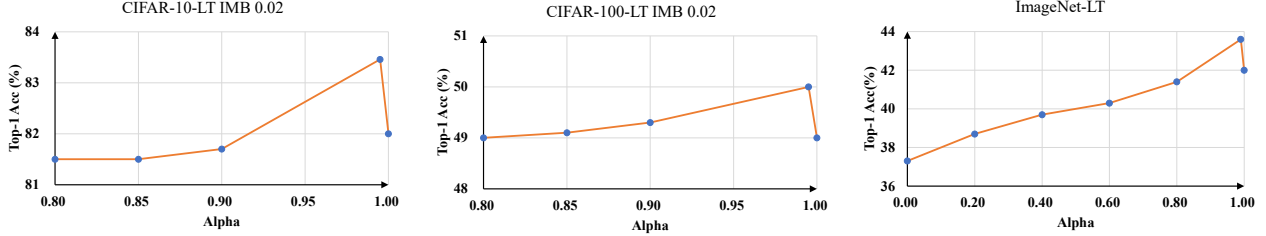


Figure 6: Effects of α on our method.

Table 5: Top-1 accuracy (%) of ResNet-32 on long-tailed CIFAR-10 and CIFAR-100 (best results are marked in bold font). † denotes results directly copied from [43]. “§” denotes the model is trained with strong data augmentation (mixup and autoaugment).

Dataset	One-stage	Long-tailed CIFAR-10			Long-tailed CIFAR-100		
		0.01	0.02	0.1	0.01	0.02	0.1
Imbalance factor	-						
Mixup [40] †	✓	73.06	77.82	87.10	39.54	44.99	58.02
Focal [23] †	✓	70.38	76.72	86.66	38.41	44.32	55.78
LDAM [5]	✓	73.35	-	86.96	39.60	-	56.91
BBN [43]	✓	79.82	82.18	88.32	42.56	47.02	59.12
CB-Focal [9] †	✓	74.57	79.27	87.10	39.60	45.17	57.99
CE+DRW [5]	✗	76.34	79.97	87.56	41.51	45.29	58.12
CE+DRS [5]	✗	75.61	79.81	87.38	41.61	45.48	58.11
LDAM+DRW [5]	✗	77.03	81.03	88.16	42.04	46.62	58.71
ELF(LDAM)+DRW [10]	✗	78.10	82.40	88.00	43.10	47.50	58.90
ResLT	✓	80.44	83.46	89.06	45.34	49.98	60.79
ResLT§	✓	82.40	85.17	89.70	48.21	52.71	62.01

Comparison on Places-LT Table 3 lists experimental results on Places-LT. Following previous setting [25, 20], we use ResNet-152 pre-trained on full ImageNet dataset as our backbone (provided by torchvision). As shown in Table 3, the model trained with our ResLT in an end-to-end manner achieves 39.8% Top-1 accuracy, which is 1.9% higher than previous SOTA [20].

Comparison on iNaturalist 2018 Experimental results on iNaturalist 2018 are summarized in Table 6. We mainly compare our method with BBN and Kang et al. [20] with 200 training epochs. Note that, though Zhou et al. [43] claimed BBN(2x) trained with 180 epochs, they actually used 360 epochs data due to their dual sampler strategy. Under the same amount of data for training, our method outperforms [43] by 0.9%. Compared with [20], our ResLT model trained in an end-to-end manner achieves 70.2% top-1 accuracy, accomplishing new state-of-the-art. Further, with larger network ResNet-152 in supplementary file, our method achieves 73.2% top-1 accuracy, surpassing [20] by 0.7%.

Table 6: Top-1 accuracy (%) on iNaturalist 2018. Rows with † denote results directly copied from [20, 43]. * denotes model is trained with 360 epochs data. “§” denotes the model is trained with mixup and initialized with ImageNet pre-trained model by torchvision.

Method	One-stage	ResNet-50
CB-Focal [9] †	✓	61.1
LDAM [5] †	✓	64.6
Baseline (CE)	✓	65.8
BBN [43] *	✓	69.6
τ -normalized [20]	✓	69.3
LDAM+DRW [5] †	✗	68.0
cRT [20]	✗	67.6
LWS [20]	✗	69.5
ResLT	✓	70.2
ResLT *	✓	70.5
LWS §	✗	71.4
ResLT §	✓	72.3

5. Conclusion

In this paper, we provide a novel perspective to understand and address the long-tailed recognition problem. The proposed residual fusion mechanism effectively re-balances head and tail classes under this new point of view in parameter space. Extensive experimental results on various representative and challenging benchmarks manifest the effectiveness of our method.

References

- [1] Mateusz Buda, Atsuto Maki, and Maciej A. Mazurowski. A systematic study of the class imbalance problem in convolutional neural networks. *Neural Networks*, 2018. 1
- [2] Mateusz Buda, Atsuto Maki, and Maciej A Mazurowski. A systematic study of the class imbalance problem in convolutional neural networks. *Neural Networks*, 2018. 1, 2
- [3] Jonathon Byrd and Zachary Lipton. What is the effect of importance weighting in deep learning? In *ICML*, 2019. 1, 2
- [4] Kaidi Cao, Colin Wei, Adrien Gaidon, Nikos Arechiga, and Tengyu Ma. Learning imbalanced datasets with label-distribution-aware margin loss. In *NeurIPS*, 2019. 3, 5, 6, 7
- [5] Kaidi Cao, Colin Wei, Adrien Gaidon, Nikos Arechiga, and Tengyu Ma. Learning imbalanced datasets with label-distribution-aware margin loss. In *NeurIPS*, 2019. 8
- [6] Nitesh V. Chawla, Kevin W. Bowyer, Lawrence O. Hall, and W. Philip Kegelmeyer. SMOTE: Synthetic minority oversampling technique. *Journal of Artificial Intelligence Research*, 2002. 1
- [7] Marius Cordts, Mohamed Omran, Sebastian Ramos, Timo Rehfeld, Markus Enzweiler, Rodrigo Benenson, Uwe Franke, Stefan Roth, and Bernt Schiele. The cityscapes dataset for semantic urban scene understanding. In *CVPR*, 2016. 1
- [8] Yin Cui, Menglin Jia, Tsung-Yi Lin, Yang Song, and Serge J. Belongie. Class-balanced loss based on effective number of samples. In *CVPR*, 2019. 1, 3
- [9] Yin Cui, Menglin Jia, Tsung-Yi Lin, Yang Song, and Serge Belongie. Class-balanced loss based on effective number of samples. In *CVPR*, 2019. 8
- [10] Rahul Duggal, Scott Freitas, Sunny Dhamnani, Duen Horng Chau, and Jimeng Sun. ELF: an early-exiting framework for long-tailed classification. *CoRR*, abs/2006.11979, 2020. 8
- [11] Spyros Gidaris and Nikos Komodakis. Dynamic few-shot visual learning without forgetting. In *CVPR*, 2018. 11
- [12] Haibo He and Edwardo A Garcia. Learning from imbalanced data. *IEEE TKDE*, 2009. 1, 2
- [13] Kaiming He, Xiangyu Zhang, Shaoqing Ren, and Jian Sun. Deep residual learning for image recognition. In *CVPR*, 2016. 1, 5, 6
- [14] Chen Huang, Yining Li, Chen Change Loy, and Xiaoou Tang. Learning deep representation for imbalanced classification. In *CVPR*, 2016. 1, 2, 3
- [15] Chen Huang, Yining Li, Change Loy Chen, and Xiaoou Tang. Deep imbalanced learning for face recognition and attribute prediction. *IEEE TPAMI*, 2019. 1, 2, 3
- [16] Chen Huang, Yining Li, Chen Change Loy, and Xiaoou Tang. Learning deep representation for imbalanced classification. In *CVPR*, 2016. 1
- [17] Muhammad Abdullah Jamal, Matthew Brown, Ming-Hsuan Yang, Liqiang Wang, and Boqing Gong. Rethinking class-balanced methods for long-tailed visual recognition from a domain adaptation perspective. In *CVPR*, 2020. 2
- [18] Nathalie Japkowicz and Shaju Stephen. The class imbalance problem: A systematic study. *Intelligent Data Analysis*, 2002. 1, 2
- [19] Buyu Li Quanquan Li Wanli Ouyang Changqing Yin Junjie Yan Jingru Tan, Changbao Wang. Equalization loss for long-tailed object recognition. In *CVPR*, 2020. 11
- [20] Bingyi Kang, Saining Xie, Marcus Rohrbach, Zhicheng Yan, Albert Gordo, Jiashi Feng, and Yannis Kalantidis. Decoupling representation and classifier for long-tailed recognition. *arXiv preprint arXiv:1910.09217*, 2019. 3, 5, 6, 7, 8, 11
- [21] Alex Krizhevsky, Ilya Sutskever, and Geoffrey E Hinton. ImageNet classification with deep convolutional neural networks. In *NeurIPS*, 2012. 1
- [22] Buyu Li, Yu Liu, and Xiaogang Wang. Gradient harmonized single-stage detector. In *AAAI*, 2019. 3
- [23] Tsung-Yi Lin, Priya Goyal, Ross Girshick, Kaiming He, and Piotr Dollár. Focal loss for dense object detection. In *ICCV*, 2017. 3, 6, 8, 11
- [24] Tsung-Yi Lin, Michael Maire, Serge Belongie, James Hays, Pietro Perona, Deva Ramanan, Piotr Dollár, and C Lawrence Zitnick. Microsoft COCO: Common objects in context. In *ECCV*, 2014. 1
- [25] Ziwei Liu, Zhongqi Miao, Xiaohang Zhan, Jiayun Wang, Boqing Gong, and Stella X. Yu. Large-scale long-tailed recognition in an open world. In *CVPR*, 2019. 5, 6, 8, 11
- [26] Mengye Ren, Wenyuan Zeng, Bin Yang, and Raquel Urtasun. Learning to reweight examples for robust deep learning. In *ICML*, 2018. 2
- [27] Shaoqing Ren, Kaiming He, Ross Girshick, and Jian Sun. Faster r-cnn: Towards real-time object detection with region proposal networks. In *NeurIPS*, 2015. 1
- [28] Olga Russakovsky, Jia Deng, Hao Su, Jonathan Krause, Sanjeev Satheesh, Sean Ma, Zhiheng Huang, Andrej Karpathy, Aditya Khosla, and Michael Bernstein. ImageNet large scale visual recognition challenge. *IJCV*, 2015. 1, 5
- [29] Li Shen, Zhouchen Lin, and Qingming Huang. Relay back-propagation for effective learning of deep convolutional neural networks. In *ECCV*, 2016. 1, 2
- [30] Jun Shu, Qi Xie, Lixuan Yi, Qian Zhao, Sanping Zhou, Zongben Xu, and Deyu Meng. Meta-weight-net: Learning an explicit mapping for sample weighting. In *NeurIPS*, 2019. 2
- [31] Karen Simonyan and Andrew Zisserman. Very deep convolutional networks for large-scale image recognition. In *ICLR*, 2015. 1

[32] Hyun Oh Song, Yu Xiang, Stefanie Jegelka, and Silvio Savarese. Deep metric learning via lifted structured feature embedding. In *CVPR*, 2016. 6, 11

[33] Christian Szegedy, Wei Liu, Yangqing Jia, Pierre Sermanet, Scott Reed, Dragomir Anguelov, Dumitru Erhan, Vincent Vanhoucke, and Andrew Rabinovich. Going deeper with convolutions. In *CVPR*, 2015. 1

[34] Kaihua Tang, Jianqiang Huang, and Hanwang Zhang. Long-tailed classification by keeping the good and removing the bad momentum causal effect. In *NeurIPS*, 2020. 3, 11

[35] Grant Van Horn, Oisin Mac Aodha, Yang Song, Yin Cui, Chen Sun, Alex Shepard, Hartwig Adam, Pietro Perona, and Serge Belongie. The iNaturalist species classification and detection dataset. In *CVPR*, 2018. 5

[36] Yu-Xiong Wang, Deva Ramanan, and Martial Hebert. Learning to model the tail. In *NeurIPS*, 2017. 2

[37] Xiu-Shen Wei, Peng Wang, Lingqiao Liu, Chunhua Shen, and Jianxin Wu. Piecewise classifier mappings: Learning fine-grained learners for novel categories with few examples. *IEEE TIP*, 2019. 5

[38] Liuyu Xiang, Guiguang Ding, and Jungong Han. Learning from multiple experts: Self-paced knowledge distillation for long-tailed classification. In *ECCV*, 2020. 6, 11

[39] Sangdoo Yun, Dongyoon Han, Seong Joon Oh, Sanghyuk Chun, Junsuk Choe, and Youngjoon Yoo. Cutmix: Regularization strategy to train strong classifiers with localizable features. In *ICCV*, 2019. 6

[40] Hongyi Zhang, Moustapha Cisse, Yann N. Dauphin, and David Lopez-Paz. mixup: Beyond empirical risk minimization. In *ICLR*, 2018. 6, 7, 8

[41] Xiao Zhang, Zhiyuan Fang, Yandong Wen, Zhifeng Li, and Yu Qiao. Range loss for deep face recognition with long-tailed training data. In *ICCV*, 2017. 6, 11

[42] Q Zhong, C Li, Y Zhang, H Sun, S Yang, D Xie, and S Pu. Towards good practices for recognition & detection. In *CVPR workshops*, 2016. 1, 2

[43] Boyan Zhou, Quan Cui, Xiu-Shen Wei, and Zhao-Min Chen. Bbn: Bilateral-branch network with cumulative learning for long-tailed visual recognition. *arXiv preprint arXiv:1912.02413*, 2019. 3, 5, 6, 7, 8

[44] Bolei Zhou, Agata Lapedriza, Aditya Khosla, Aude Oliva, and Antonio Torralba. Places: A 10 million image database for scene recognition. *IEEE TPAMI*, 2018. 1, 5, 6

ResLT: Residual Learning for Long-tailed Recognition

Supplementary Material

A. More Comparison with Previous Methods on ImageNet-LT.

Many previous methods mainly conduct experiments on ImageNet-LT with ResNet-10 architecture. Here we show more comparisons with these works. The summary is shown in Table 7.

Table 7: More comparisons on ImageNet-LT with ResNet-10. Top-1 accuracies (%) are reported.

Method	One-stage	Many	Medium	Few	All
FSLwF [11]	✓	40.9	22.1	15.0	28.4
Focal Loss [23] †	✓	36.4	29.9	16.0	30.5
Range Loss [41] †	✓	35.8	30.3	17.6	30.7
Lifted Loss [32] †	✓	35.8	30.4	17.9	30.8
SEQL [19]	✓	49.4	32.2	14.5	36.4
τ -normalize [20]	✓	50.4	42.1	26.7	42.7
LFME [38]	✗	47.0	37.9	19.2	38.8
OLTR [25]	✗	43.2	35.1	18.5	35.6
cRT [20]	✗	53.8	41.3	25.4	43.2
LWS [20]	✗	51.8	41.6	27.6	43.0
ResLT	✓	52.3	41.6	29.5	43.8

B. Comparison with the Concurrent Method on ImageNet-LT.

Table 8: Top-1 accuracy (%) on ImageNet-LT for ResNeXt-50. † denotes results directly copied from [34]. We use their open-source code to conduct experiments under 180 epochs.

Method	One-stage	Many	Medium	Few	All
De-confound [34] †	✓	67.9	42.7	14.7	48.6
De-confound-TDE [34] †	✓	62.7	48.8	31.6	51.8
De-confound [34] (180 epochs)	✓	67.4	43.0	17.2	48.9
De-confound-TDE [34] (180 epochs)	✓	64.9	48.0	28.9	51.9
ResLT	✓	63.0	50.5	35.5	52.9

C. More Experimental Results on Many-shot, Medium-shot, and Few-shot.

Table 9: Comprehensive results on ImageNet-LT with different backbone networks (ResNet-10, ResNeXt-50 & ResNeXt-101) under 180 epochs training.

Backbone	Method	Many	Medium	Few	All
ResNet-10	CE (baseline)	59.7	29.4	5.7	37.3
	cRT	53.8	41.3	25.4	43.2
	τ -normalize	50.4	42.1	26.7	42.7
	LWS	51.8	41.6	27.6	43.0
	ResLT	52.3	41.6	29.5	43.8
ResNeXt-50	CE (baseline)	66.8	42.0	14.0	47.0
	cRT	63.7	47.6	28.3	50.6
	τ -normalize	62.3	48.9	33.7	51.5
	LWS	63.3	48.4	32.0	51.5
	ResLT	63.0	50.5	35.5	52.9
ResNeXt-101	CE (baseline)	69.6	44.6	15.6	49.6
	cRT	69.0	66.0	63.2	65.2
	τ -normalize	65.3	51.5	35.2	53.9
	LWS	65.7	51.4	34.7	54.0
	ResLT	63.3	53.3	40.3	55.1

Table 10: Comprehensive results on iNaturalist 2018 with ResNet-50/152 under 200 epochs training. "§" denotes the model is trained with mixup and initialized with ImageNet pre-trained model by torchvision.

Backbone	Method	Many	Medium	Few	All
ResNet-50	CE (baseline)	75.7	66.9	61.7	65.8
	cRT	73.2	68.8	66.1	68.2
	τ -normalize	71.1	68.9	69.3	69.3
	LWS	71.0	69.8	68.8	69.5
	ResLT	68.5	69.9	70.4	70.2
ResNet-152	CE (baseline)	78.2	70.6	64.7	69.0
	cRT	75.9	71.9	69.1	71.2
	τ -normalize	74.3	72.3	72.2	72.5
	LWS	74.3	72.4	71.2	72.1
	ResLT	72.4	73.3	72.9	73.2
ResNet-50 §	CE (baseline)	78.3	69.5	63.7	67.8
	τ -normalize	71.6	70.8	71.1	71.0
	LWS	73.4	72.5	70.2	71.4
	ResLT	71.7	72.5	72.1	72.3